RSC Advances

PAPER

View Article Online
View Journal | View Issue

Cite this: *RSC Adv.*, 2018, **8**, 8412

A study on enhancing the quantum yield and antimicrobial activity of Pr(III) by varying the coordination environment†

Iffat Ameen, Abhishek Kumar Tripathi, Raj Laxmi Mishra, Afshan Siddiqui and Umesh Nath Tripathi *

Received 4th December 2017
Accepted 10th February 2018

DOI: 10.1039/c7ra13035j

rsc.li/rsc-advances

Praseodymium forms complexes easily with nitrogen and oxygen donor pyrazolines and also forms mixed ligand complexes with these pyrazolines and sulfur donor thio ligands such as dithiocarbamates and xanthates. These newly synthesized complexes have been characterized using elemental analysis, FTIR, TGA, SEM, TEM, PXRD and UV-visible spectral measurements. The isotopic studies were performed using DART mass spectrometry. The luminescent properties of these types of complexes were studied using a fluorescence spectrophotometer. The antimicrobial behavior of these praseodymium complexes was studied thoroughly during the present research.

1 Introduction

The complexes of luminescent trivalent lanthanide ions[1–3] have been studied because of the wide range of their applications in various fields. The biological activity of lanthanide complexes are also well reported in literature.[4–9] Papers in the literature reveal that praseodymium (Pr) complexes have higher antimicrobial activity than the corresponding Schiff base ligands.[10,11] The complexes of Pr were also tested against Gram positive and Gram negative bacteria using serial dilution techniques and it was found to have greater activity against the Gram positive bacterium *Staphylococcus aureus*, whereas the activity against the Gram negative bacterium *Escherichia coli* was somewhat inhibited when compared to the effects of the ligand tetracycline.[12] That this statement is contradictory was proven by Pusz *et al.*, who showed that enhanced antibacterial activity was found against the Gram negative bacteria, *E. coli* and the antibacterial activity was inhibited with a Gram positive bacteria, *Enterococcus hirae* when compared to their respective ligands.[13] Geethalaksmi and Theivarasu studied the antibacterial activities of Pr(III) complexes against two Gram positive bacteria (*S. aureus*, *Bacillus subtilis*), two Gram negative bacteria (*E. coli*, *Pseudomonas aeruginosa*) bacteria and also the fungal activity against *Candida albicans* and *Aspergillus niger*, with reference to their ligand and standard drugs. The Pr(III) complexes showed greater activity than the corresponding ligands and somewhat less activity than the standard antibacterial drug ciprofloxacin. These Pr complexes also have higher antifungal activity than the corresponding ligand and lower activity than the standard drug clotrimazole but for the fungus, *C. albicans* their antifungal activity is greater than the ligand as well as the standard antifungal drug.[14] Rare-earth metals are also known luminescent materials for use in multicolor electroluminescence and cathodoluminescence devices.[15] Because the lanthanide [Ln(III)] complexes exhibit intense luminescence, a wide range of applications become possible, mainly for near-infrared (NIR) lanthanide emitters such as samarium [Sm(III)], dysprosium [Dy(III)], praseodymium [Pr(III)], holmium [Ho(III)], ytterbium [Yb(III)], neodymium [Nd(III)], and erbium [Er(III)].[15–24] For example, NIR luminescence from ions such as Pr(III) and Er(III) are very useful when applied in telecommunication network optical signal amplifiers.[25,26]

Among rare-earth ions, the Pr ion has many possible applications because of its large number of absorption bands in the UV-visible and NIR regions, which show the possibility for simultaneous emission in the blue, green, orange, red, and infrared regions.[27] Pr^{3+}-doped glasses and crystals have been developed for applications such as optical amplifiers, up-converters, and opto-electronic devices,[28–31] mainly for fiber-based optical communication systems.[32] The absorption spectra of rare-earth metal ions consisting of sharp bands from electronic transitions within the f^n configuration, are generally slightly affected by the change in environment of the metal ion. However, if the strength of the ionic field changes, some absorption peaks may be shifted in wavelength and intensity.[33] For over a decade, Pr(III) ions, which belong to the main red emissive components for fluorescence materials, have been widely used as the luminescence activators for long afterglow

Department of Chemistry, D. D. U. Gorakhpur University, Gorakhpur, U. P, India. E-mail: un_tripathi@yahoo.com; Tel: +91-9455670369

† Electronic supplementary information (ESI) available. See DOI: 10.1039/c7ra13035j

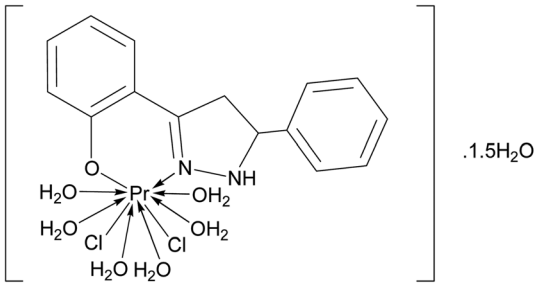

Fig. 1 Tentative structure of $[Pr(C_{15}H_{12}N_2OH)(6H_2O)Cl_2]\cdot 1.5H_2O$.

because of its profusely luminous colors.[34–36] Almost all of the $4f^2$ levels can be obtained by the absorption of one photon in the visible or IR range.[37]

In this paper, the intense red/orange emission of Pr(III) from the $^3P_0$–$^3H_4$ transition and its antimicrobial activity is reported. These two properties of Pr(III) complexes can be tuned to give an important application in the medicinal field of tracing drugs. There are already a number of papers in the literature which present the luminescence behavior of the pyrazoline ligand itself,[38–46] and therefore, this study is important as it describes the effect of various ligands on the quantum yield of Pr. The luminescence behavior of these complexes was expected to change by varying ligands around the central metal ion. Thus, the present paper reports the synthesis of new fluorescent Pr(III) complexes and their antimicrobial activities.

2 Experimental

Solvents (benzene, methanol, ethanol and so on) were rigorously dried and purified using standard methods before use.[47] All chemicals were of analytical grade quality. Praseodymium(III) chloride hexahydrate ($PrCl_3\cdot 6H_2O$; High Purity Laboratory Chemicals, India), diethyldithiocarbamate (SD Fine Chemicals, India), *o*-hydroxyacetophenone (CDH Chemicals, India) and benzaldehydes (E. Merck) were used as received. Pyrazolines were prepared using a previously reported method.[48,49]

2.1 Synthesis of $[Pr(C_{15}H_{12}N_2OX)Cl_2\cdot nH_2O]$

The complexes of Pr(III) with 3(2′-hydroxyphenyl)-5-(4-substituted phenyl) pyrazolines with the general formula $[Pr(C_{15}H_{12}N_2OX)Cl_2\cdot nH_2O]$ were prepared using the following reaction scheme in a 1 : 1 molar ratio (Fig. 1).

$$PrCl_3\cdot 6H_2O + (C_{15}H_{12}N_2OX)Na \rightarrow [Pr(C_{15}H_{15}N_2OX)Cl_2\cdot nH_2O] + NaCl$$

2.1.1 Procedure. Small pieces of sodium were placed in a flask with excess of isopropanol and refluxed for 30 min, to obtain a clear solution of sodium isopropoxide. The benzene solution of 3(2′-hydroxyphenyl)-5-(4-substituted phenyl) pyrazoline was then added and the reaction mixture was further refluxed for about 30 min, until a constant yellow color solution was obtained. The reaction mixture was cooled to room temperature and then a methanolic solution of metal chloride was added with constant stirring. The content was further stirred at room temperature for about two hours, until the color of the reaction mixture underwent a visible change. The reaction mixture was filtered to remove the precipitated sodium chloride (NaCl). The solvent was removed from the filtrate under reduced pressure and a yellow colored solid was obtained. Compounds 1–4 were prepared by this method. The physical details are given in Table 1.

2.2 Synthesis of mixed ligand complexes of the type $[Pr(C_5H_{10}NS_2)(C_{15}H_{12}N_2OX)Cl\cdot nH_2O]$ and $[Pr(C_2H_5OCS_2)(C_{15}H_{12}N_2OX)Cl\cdot nH_2O]$

The mixed ligand complexes of Pr were prepared using the following two steps:

Step 1:

$$PrCl_36H_2O + C_{15}H_{13}N_2OX \rightarrow [Pr(C_{15}H_{12}N_2OX)Cl_2\cdot nH_2O] + HCl$$

Step 2:

$$[Pr(C_{15}H_{12}N_2OX)Cl_2\cdot nH_2O] + Na(C_5H_{10}NS_2)\cdot 3H_2O \rightarrow [Pr(C_{15}H_{12}N_2OX)(C_5H_{10}NS_2)Cl\cdot nH_2O] + NaCl \quad (I)$$

$$[Pr(C_{15}H_{12}N_2OX)Cl_2\cdot nH_2O] + K(C_2H_5OCS_2)\cdot 3H_2O \rightarrow [Pr(C_{15}H_{12}N_2OX)(C_2H_5OCS_2)Cl\cdot nH_2O] + KCl \quad (II)$$

Table 1 Physical characterization details of the praseodymium complexes under investigation

Comp. no.	Compounds	Yield (%)	Mp (°C)	Mol. wt. found (calc'd)	Physical state/colour
1	$[Pr(C_{15}H_{12}N_2O\cdot H)(6H_2O)Cl_2]\cdot 1.5H_2O$	89	188	585.68 (584.21)	Amorphous/yellow
2	$[Pr(C_{15}H_{12}N_2O\cdot OCH_3)(6H_2O)Cl_2]\cdot 1.5H_2O$	86	189	615.81 (614.24)	Amorphous/yellow
3	$[Pr(C_{15}H_{12}N_2O\cdot CH_3)(6H_2O)Cl_2]\cdot 1.5H_2O$	90	194	599.96 (598.24)	Amorphous/yellow
4	$[Pr(C_{15}H_{12}N_2O\cdot Cl)(6H_2O)Cl_2]\cdot 1.5H_2O$	82	194	621.87 (618.66)	Amorphous/yellow
5	$[Pr(C_5H_{10}NS_2)(C_{15}H_{12}N_2O\cdot H)(3H_2O)Cl]$	88	210	617.33 (615.95)	Amorphous/yellow
6	$[Pr(C_5H_{10}NS_2)(C_{15}H_{12}N_2O\cdot OCH_3)(3H_2O)Cl]$	92	212	647.01 (645.98)	Amorphous/yellow
7	$[Pr(C_5H_{10}NS_2)(C_{15}H_{12}N_2O\cdot CH_3)(3H_2O)Cl]$	91	215	631.25 (629.98)	Amorphous/yellow
8	$[Pr(C_5H_{10}NS_2)(C_{15}H_{12}N_2O\cdot Cl)(3H_2O)Cl]$	89	218	653.62 (650.40)	Amorphous/yellow
9	$[Pr(C_2H_5OCS_2)(C_{15}H_{12}N_2O\cdot H)(2H_2O)Cl]\cdot H_2O$	87	233	589.98 (588.88)	Amorphous/yellow
10	$[Pr(C_2H_5OCS_2)(C_{15}H_{12}N_2O\cdot OCH_3)(2H_2O)Cl]\cdot H_2O$	85	232	620.24 (618.91)	Amorphous/yellow
11	$[Pr(C_2H_5OCS_2)(C_{15}H_{12}N_2O\cdot CH_3)(2H_2O)Cl]\cdot H_2O$	84	237	603.99 (602.91)	Amorphous/yellow
12	$[Pr(C_2H_5OCS_2)(C_{15}H_{12}N_2O\cdot Cl)(2H_2O)Cl]\cdot H_2O$	86	235	626.64 (623.33)	Amorphous/yellow

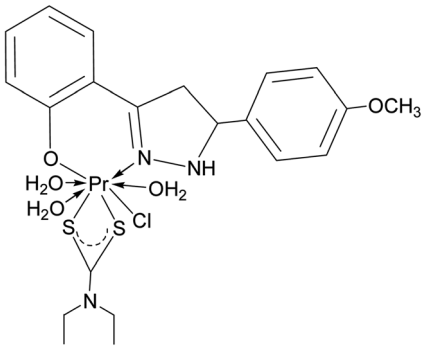

Fig. 2 Tentative structure of $[Pr(C_5H_{10}NS_2)(C_{15}H_{12}N_2O\cdot OCH_3)(3H_2O)Cl]$.

2.2.1 Procedure. A methanolic solution of metal chloride was added to a benzene solution of 3(2′-hydroxyphenyl)-5-(4-substituted phenyl) pyrazoline and refluxed for 5–6 h (Step 1). The color of the solution became yellow. The solution was cooled at room temperature and a methanolic solution of sodium diethyldithiocarbamate (Step 2, I) or potassium ethyl xanthate (Step 2, II) was added. The solution was stirred at room temperature for about 10 h. The solvent was removed under vacuum to ensure a good yield and purity. The yellow colored solid obtained was washed with water and dried at 80 °C. Compounds 5–12 were also prepared using this method (Fig. 2 and 3). The physical details are given in Table 1.

2.3 Antimicrobial assay

The antibacterial and antifungal activities of some of the representative complexes: 2, 6 and 10 were determined and the results obtained were compared with those obtained using tetracycline and fluconazole. The antimicrobial studies were carried out using a prepared solution with a concentration of 2.5 mg mL^{-1}. The study of the antibacterial and antifungal activity was carried out using the antibiotic sensitivity test (disc diffusion method).[50,51] The pathogens, against which antibacterial activity was observed, were *E. coli* MTCC 1687, *P. aeruginosa* MTCC 741, *S. aureus* MTCC 902 and antifungal activity was observed against *C. albicans* MTCC 3017 and *A. niger* MTCC 404. The antibacterial and antifungal activities of these complexes were compared with their respective ligands, metal chlorides and with other complexes of Pr and known antibacterial/antifungal drugs.

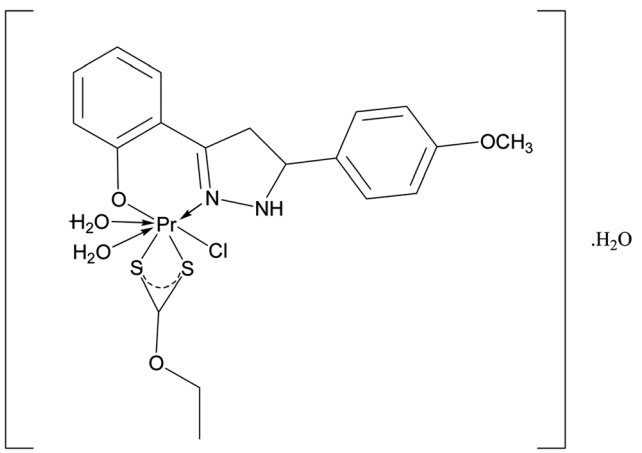

Fig. 3 Tentative structure of $[Pr(C_2H_5OCS_2)(C_{15}H_{12}N_2O\cdot OCH_3)(2H_2O)Cl]\cdot H_2O$.

2.4 Physical measurements

For the determination of molecular weights and isotopic confirmation, the molecular ion peak was detected using direct analysis in real time (DART) mass spectrometry on a JMS-T100LC AccuTOF (Jeol) mass spectrometer. The accelerating voltage was 10 kV and spectra were recorded at room temperature. Elemental analysis (C, H, N and S) was carried out on a Vario EL III cube C, H, N, S analyzer (Elementar). Oxygen was determined using an elemental analyzer (EuroVector). Chlorine was estimated using Volhard's method.[52] Praseodymium was estimated as praseodymium oxide (Pr_2O_3) using an analytical method reported by Rodden.[53] IR spectra were recorded on a model 6700 spectrophotometer (Thermo Nicolet) in the range of 5000–50 cm^{-1}. Electronic spectra were recorded in dichloromethane solution on a Cary 5000 UV-visible-NIR spectrophotometer (Agilent Technologies) within the range 2500–200 nm. SEM studies were carried out on JSM-6390LV (Jeol) at magnifications from 5× to 300 000× (both high and low vacuum models). Powder X-ray diffraction studies were carried out using an AXS D8 Advance (Bruker) diffractometer at a temperature range from −170 °C to +450 °C. Thermogravimetric analysis of the compounds was carried out using a thermogravimetric analyzer (PerkinElmer). Luminescence studies were performed using a FluoroLog spectrofluorimeter (Jobin Yvon) in the 200 nm to 700 nm range. A fluorocube lifetime spectrofluorometer system (Jobin-Yvon) was used to measure the lifetime fluorescence.

3 Results and discussion

All the synthesized Pr complexes were yellow colored amorphous solids, non-hygroscopic, stable at room temperature and soluble in solvents such as dimethylformamide, dichloromethane and so on. Molecular weight measurements showed that these complexes were monomeric in nature. The elemental analysis (C, H, N, S, O, Cl and Pr) data were in agreement with the stoichiometry proposed, which is given in Table 2.

3.1 FTIR spectral data

The IR spectral data of these Pr(III) complexes showed bands in the regions 3401–3336, 1609–1600, 451–433, 396–367, 346–330 cm^{-1} which were assigned to ν(N–H), ν(C=N), ν(Pr–O), ν(Pr–N), ν(Pr–S)[54–63] as shown in Table 3. A broad band for $[Pr(C_{15}H_{12}N_2OX)Cl_2\cdot nH_2O]$ $[Pr(C_5H_{10}NS_2)(C_{15}H_{12}N_2OX)Cl\cdot nH_2O]$ and $[Pr(C_2H_5OCS_2)(C_{15}H_{12}N_2OX)Cl\cdot nH_2O]$ at 3433–3411 cm^{-1} was assigned to ν(O–H).[61] The appearance of a ν(O–H) stretching band suggested the presence of water in these complexes which was also confirmed by the TGA/(differential

Table 2 Elemental analysis data of the complexes

Comp. no.	Compound	% C found (calc'd)	% H found (calc'd)	% N found (calc'd)	% S found (calc'd)	% Cl found (calc'd)	% O found (calc'd)	% Pr Found (calc'd)
1	$[Pr(C_{15}H_{12}N_2O\cdot H)(6H_2O)Cl_2]\cdot 1.5H_2O$	30.91 (30.83)	4.93 (4.91)	4.76 (4.79)	—	12.36 (12.31)	23.34 (23.27)	23.92 (24.12)
2	$[Pr(C_{15}H_{12}N_2O\cdot OCH_3)(6H_2O)Cl_2]\cdot 1.5H_2O$	31.40 (31.28)	5.07 (5.04)	4.54 (4.56)	—	11.52 (11.54)	23.69 (24.74)	22.74 (22.94)
3	$[Pr(C_{15}H_{12}N_2O\cdot CH_3)(6H_2O)Cl_2]\cdot 1.5H_2O$	32.13 (32.03)	5.15 (5.12)	5.22 (5.20)	—	11.85 (11.81)	22.70 (22.66)	23.26 (23.48)
4	$[Pr(C_{15}H_{12}N_2O\cdot Cl)(6H_2O)Cl_2]\cdot 1.5H_2O$	29.06 (29.12)	4.46 (4.48)	4.55 (4.52)	—	17.22 (17.19)	22.05 (21.98)	22.63 (22.77)
5	$[Pr(C_5H_{10}NS_2)(C_{15}H_{12}N_2O\cdot H)(3H_2O)Cl]$	39.14 (39.00)	4.78 (4.75)	6.79 (6.82)	10.45 (10.41)	5.78 (5.76)	10.35 (10.39)	22.74 (22.88)
6	$[Pr(C_5H_{10}NS_2)(C_{15}H_{12}N_2O\cdot OCH_3)(3H_2O)Cl]$	39.14 (39.05)	4.85 (4.84)	6.53 (6.50)	9.96 (9.93)	5.52 (5.49)	12.41 (12.38)	21.66 (21.81)
7	$[Pr(C_5H_{10}NS_2)(C_{15}H_{12}N_2O\cdot CH_3)(3H_2O)Cl]$	39.98 (40.04)	4.99 (4.96)	6.69 (6.67)	10.21 (10.18)	5.60 (5.63)	10.13 (10.16)	22.30 (22.37)
8	$[Pr(C_5H_{10}NS_2)(C_{15}H_{12}N_2O\cdot Cl)(3H_2O)Cl]$	37.05 (36.93)	4.37 (4.34)	6.49 (6.46)	9.82 (9.86)	10.98 (10.90)	9.86 (9.84)	21.46 (21.66)
9	$[Pr(C_2H_5OCS_2)(C_{15}H_{12}N_2O\cdot H)(2H_2O)Cl]\cdot H_2O$	36.83 (36.71)	4.08 (4.11)	4.74 (4.76)	10.93 (10.89)	6.04 (6.07)	13.62 (13.58)	23.78 (23.93)
10	$[Pr(C_2H_5OCS_2)(C_{15}H_{12}N_2O\cdot OCH_3)(2H_2O)Cl]\cdot H_2O$	36.86 (36.87)	4.26 (4.23)	4.54 (4.53)	10.40 (10.36)	5.70 (5.73)	15.56 (15.51)	22.69 (22.77)
11	$[Pr(C_2H_5OCS_2)(C_{15}H_{12}N_2O\cdot CH_3)(2H_2O)Cl]\cdot H_2O$	37.92 (37.85)	4.36 (4.35)	4.67 (4.65)	10.60 (10.64)	5.85 (5.88)	13.30 (13.27)	23.31 (23.37)
12	$[Pr(C_2H_5OCS_2)(C_{15}H_{12}N_2O\cdot Cl)(2H_2O)Cl]\cdot H_2O$	34.70 (34.68)	3.71 (3.72)	4.51 (4.49)	10.32 (10.29)	11.42 (11.38)	12.79 (12.83)	22.52 (22.61)

thermal analysis) DTG data. The Fourier-transform-infrared (FTIR) spectral peaks of complexes 6 and 10 are given as ESI [Fig. S1(a) and (b)†].

3.2 Pyrolysis behavior of praseodymium complexes

The synthesized Pr complexes were stable at room temperature but on applying heat, they showed a continuous weight loss. The thermal behavior of these Pr complexes was examined using TGA, DTG and differential thermal analysis (DTA) techniques. The TGA and DTG analyses were carried out in a nitrogen (N_2) atmosphere, whereas the DTA was carried out in an oxygen (O_2) atmosphere to observe the effect of O_2 on the decomposition temperature. The decomposition patterns of some representative complexes are given in Table 4.

Using TGA and DTG curves, the first dehydration of Pr complexes 1 and 10 occurred between 85–100 °C, which can be attributed to the presence of crystallized water.[64,65] This type of broad peak is absent in complex 6 which shows a lack of crystallized water. The percentage weight loss obtained using TGA and the peaks present found using DTG confirms the amount of coordinated water molecules present in these complexes. The coordinated water molecules are generally decomposed between 200–220 °C in mixed ligand complexes 6 and 10, whereas the complex 1 loses its coordinated water at around 350 °C. This behavior of decomposition can be justified by the steric hindrance because of the presence of two types of bidentate ligands, which weakens the water–praseodymium coordinate bond, and thus, the mixed ligand complexes easily liberate their coordinated water. The decomposition of the sulfur containing organic moiety can be seen in the temperature range: 310–330 °C, whereas the nitrogen and oxygen containing organic species decompose at temperatures above 600 °C. Because the bond dissociation energy of Pr–O (796 kJ mol^{-1}) is higher than that of the Pr–S (423 kJ mol^{-1}), this is the reason for the dissociation of sulfur containing organic occurring earlier than the oxygen containing one. Because complex 1 has only one type of ligand in its coordination sphere, the decomposition and oxidation of the organic moiety[64,66–68] from the anhydrous Pr complexes and oxidation of the Pr in Pr_2O_3 occurred in one single step in these complexes, whereas in complex 6 and 10 these processes occur in two steps because of the presence of two types of coordinated ligands in these types of mixed ligand complexes of Pr.

The DTA curves of all of these three types of complexes follow the same pattern. A broad endothermic peak at temperature 130 °C confirms the dehydration of the Pr complexes. The exothermic peak around 420 °C indicates the bond formation when the oxidation of the organic moiety occurs. The temperature difference between the TGA-DTG and differential scanning calorimetry (DSC) incidence can be explained using reports in the literature[69–71] which reveal that the oxidizing atmosphere accelerates the thermal decomposition. Excluding this there is no other clear result obtained from the DTA curve. The decomposition pattern and effect of temperature can be seen in Fig. 4(a)–(c).

Table 3 FTIR spectral data of the complexes

Comp. no.	Compounds	ν(O–H)	ν(N–H)	ν(C=N)	ν(Pr–O)	ν(Pr–N)	ν(Pr–S)
1	$[Pr(C_{15}H_{12}N_2O{\cdot}H)(6H_2O)Cl_2]{\cdot}1.5H_2O$	3422	3382	1600	433	396	—
2	$[Pr(C_{15}H_{12}N_2O{\cdot}OCH_3)(6H_2O)Cl_2]{\cdot}1.5H_2O$	3418	3376	1606	436	381	—
3	$[Pr(C_{15}H_{12}N_2O{\cdot}CH_3)(6H_2O)Cl_2]{\cdot}1.5H_2O$	3436	3386	1604	444	383	—
4	$[Pr(C_{15}H_{12}N_2O{\cdot}Cl)(6H_2O)Cl_2]{\cdot}1.5H_2O$	3421	3394	1609	447	367	—
5	$[Pr(C_5H_{10}NS_2)(C_{15}H_{12}N_2O{\cdot}H)(3H_2O)Cl]$	3432	3396	1605	444	388	331
6	$[Pr(C_5H_{10}NS_2)(C_{15}H_{12}N_2O{\cdot}OCH_3)(3H_2O)Cl]$	3433	3360	1606	438	380	333
7	$[Pr(C_5H_{10}NS_2)(C_{15}H_{12}N_2O{\cdot}CH_3)(3H_2O)Cl]$	3420	3342	1603	450	382	339
8	$[Pr(C_5H_{10}NS_2)(C_{15}H_{12}N_2O{\cdot}Cl)(3H_2O)Cl]$	3429	3401	1607	446	362	330
9	$[Pr(C_2H_5OCS_2)(C_{15}H_{12}N_2O{\cdot}H)(2H_2O)Cl]{\cdot}H_2O$	3419	3369	1609	450	363	346
10	$[Pr(C_2H_5OCS_2)(C_{15}H_{12}N_2O{\cdot}OCH_3)(2H_2O)Cl]{\cdot}H_2O$	3426	3352	1606	442	376	342
11	$[Pr(C_2H_5OCS_2)(C_{15}H_{12}N_2O{\cdot}CH_3)(2H_2O)Cl]{\cdot}H_2O$	3411	3336	1603	451	380	330
12	$[Pr(C_2H_5OCS_2)(C_{15}H_{12}N_2O{\cdot}Cl)(2H_2O)Cl]{\cdot}H_2O$	3428	3392	1604	448	394	337

3.3 Absorption spectral studies

The electronic spectral data of complex 1 shows absorption at 277 nm, which indicates the ligand to metal charge transfer phenomenon.[72,73] The rest of the peaks at 1167, 1360, 1698, and 1924 nm represent the f–f transitions of Pr of $^3H_4$–$^1G_4$, $^3H_4$–$^3F_4$, $^3H_4$–$^3F_3$, $^3H_4$–$^3F_2$, respectively.[72–74] Similarly, the mixed ligand complexes show the charge transfer band at 326 nm indicating the ligand to metal charge transfer and another peak at 382 nm resembles the metal to ligand charge transfer in complex 6. In the same way, in complex 10, the ligand to metal charge transfer occurs at 357 nm whereas the metal to ligand charge transfer peak was found at 377 nm.[73,74] From Fig. 5(a)–(c), it can be seen that the metal to ligand charge transfer peak is distinct only in the complexes having sulfur donor ligand, whereas, in complex 1, which has only nitrogen and oxygen donor atoms, both of these peaks were merged. The f–f transition bands of these complexes appearing at 1207 and 1205, 1399 and 1410, 1699 and 1702, 1952 and 1940 nm may be assigned to the transition of $^3H_4$–$^1G_4$, $^3H_4$–$^3F_4$, $^3H_4$–$^3F_3$, $^3H_4$–$^3F_2$, respectively, of Pr.[74–76] The absorbance spectra with respect to transmittance and reflectance are given in the ESI [Figure S2(a)–(c)†].

3.4 Photo-physical studies

The emission spectra of these newly synthesized Pr complexes were measured in dichloromethane. These complexes emitted luminescence from two excited states, *i.e.*, $^3P_0$ and $^1D_2$ in solution.[77,78] But because the energy gap for the $^1D_2$ state is much larger than that for the other levels, it might, therefore, be expected that the emission of Pr will occur only from the $^1D_2$ state.[79]

A very high intensity peak at 604 nm in complex 6 which resembles the transition, originates from the $^1D_2$ level, whereas in complex 10 this transition occurs at 603 nm in the form of a broad peak. No such peak is obtained in complex 1. This can be justified by the quenching of their excited states by non-radiative relaxation pathways.[80,81] Multiphonon luminescence quenching in complex 1 could be upheld by the presence of a large number of water molecules in the coordination sphere.[82] Because of the involvement of six water molecules present in these complexes, $^3P_0$–$^3H_6$ transition was also suppressed.[77] A very small peak at 643 nm obtained in complex 10 corresponds to $^3P_0$–$^3F_2$ transition[77] and this may result because of the reduced number of water molecules around the metal. This peak resembles the red emission from the Pr complexes.[76] Some very low intensity peaks at 528, 493, 482 and 468 nm were obtained for complex 10. These emissions can be attributed to the radiative transition from the upper $^3P_0$ level to the lower energy states.[77,78] These radiative transition peaks at 465 and 389 nm were also seen in complex 1. The Pr complexes also emit UV 5d-4f luminescence.[77,83,84] As shown in Fig. 6(a)–(c) these peaks are found at 279 nm and 312 nm (1), 350 nm (6) and 390 nm (10). The peak with a very high intensity at 604 nm in complex 6, indicates its strong orange emission of light, whereas this emission is very weak in complex 10. There are some other blue colored light emissions in complex 1 and 10 at 469 nm (1), 468, 481, 492 nm (10), which correspond to the transition from the $^3P_0$–$^3H_4$ state.[76,85,86]

The solid state fluorescence studies were also done to observe the effect of solution on the fluorescence property of Pr complexes. On comparison it was found that the complexes had nearly the same ligand environment around the central metal atom. Almost all the emission can be seen in the given spectra. There is change only in the intensity of the peaks. The solid state fluorescence spectra are shown in the ESI [Fig. S3(a)–(c)†].

The life time decay rate (measured in dichloromethane at room temperature) showed a single exponential decay [Fig. 7(a)–(c)]. The quantum yields were calculated using the absorption and emission maxima. The radiative decay rate (K_r) and non-radiative decay rate (K_{nr}) were calculated using the life time and emission quantum yields. In complex 1 and 10 K_r was much larger than K_{nr}, which reveals its radiative emission in good extent. Complex 6 had approximately equal values of K_r and K_{nr} with 55% quantum efficiency, which agrees with the fact that approximately 50% of the absorbed energy, was released in the form of light and 50% was liberated as phonons. The life time of this complex was about 74.48 ns. A large Stoke's shift and comparatively large band gap also contribute to this phenomenon. Comparatively lower K_r, and K_{nr}, high quantum efficiency (approximately 91%), small Stoke's shift and lower energy band gap show that there was a strong overlap between the S_0 and S_1 state in complex 10 and this could be the reason for the highest emission life time. The enhanced life time of

Table 4 Thermogravimetric analysis data of the complexes

Comp. no.	Compound	Temperature (°C)	Weight loss found (calc'd)	Fragment lost
1	$[Pr(C_{15}H_{12}N_2O\cdot H)(6H_2O)Cl_2]\cdot 1.5H_2O$	98	4.62 (4.38)	$-1.5H_2O$
		192	11.96 (12.15)	$-2Cl$
		336	18.02 (18.48)	$-6H_2O$
		625	39.21 (40.56)	$-C_{15}H_{12}N_2OH$
2	$[Pr(C_{15}H_{12}N_2O\cdot OCH_3)(6H_2O)Cl_2]\cdot 1.5H_2O$	102	4.03 (4.39)	$-1.5H_2O$
		189	10.28 (11.55)	$-2Cl$
		340	18.17 (17.58)	$-6H_2O$
		628	43.97 (43.51)	$-C_{15}H_{12}N_2O\cdot OCH_3$
3	$[Pr(C_{15}H_{12}N_2O\cdot CH_3)(6H_2O)Cl_2]\cdot 1.5H_2O$	99	4.11 (4.51)	$-1.5H_2O$
		196	11.67 (11.86)	$-2Cl$
		338	18.81 (18.05)	$-6H_2O$
		630	42.34 (42.00)	$-C_{15}H_{12}N_2O\cdot CH_3$
4	$[Pr(C_{15}H_{12}N_2O\cdot Cl)(6H_2O)Cl_2]\cdot 1.5H_2O$	96	4.84 (4.36)	$-1.5H_2O$
		200	11.24 (11.46)	$-2Cl$
		334	17.69 (17.45)	$-6H_2O$
		633	43.19 (43.92)	$-C_{15}H_{12}N_2OCl$
5	$[Pr(C_5H_{10}NS_2)(C_{15}H_{12}N_2O\cdot H)(3H_2O)Cl]$	176	5.89 (5.76)	$-Cl$
		215	8.00 (8.76)	$-3H_2O$
		336	24.96 (24.07)	$-C_5H_{10}NS_2$
		634	39.50 (38.52)	$-C_{15}H_{12}N_2OH$
6	$[Pr(C_5H_{10}NS_2)(C_{15}H_{12}N_2O\cdot OCH_3)(3H_2O)Cl]$	163	5.31 (5.49)	$-Cl$
		218	8.74 (8.35)	$-3H_2O$
		345	23.33 (22.95)	$-C_5H_{10}NS_2$
		620	42.69 (41.37)	$-C_{16}H_{15}N_2O_2$
7	$[Pr(C_5H_{10}NS_2)(C_{15}H_{12}N_2O\cdot CH_3)(3H_2O)Cl]$	180	5.44 (5.63)	$-Cl$
		222	8.02 (8.57)	$-3H_2O$
		329	24.10 (23.53)	$-C_5H_{10}NS_2$
		634	41.00 (39.89)	$-C_{16}H_{15}N_2O$
8	$[Pr(C_5H_{10}NS_2)(C_{15}H_{12}N_2O\cdot Cl)(3H_2O)Cl]$	175	5.30 (5.45)	$-Cl$
		225	8.19 (8.30)	$-3H_2O$
		324	23.64 (22.79)	$-C_5H_{10}NS_2$
		636	42.31 (41.77)	$-C_{15}H_{12}N_2OCl$
9	$[Pr(C_2H_5OCS_2)(C_{15}H_{12}N_2O\cdot H)(2H_2O)Cl]\cdot H_2O$	85	3.24 (3.05)	$-H_2O$
		198	6.69 (6.08)	$-Cl$
		200	6.94 (6.11)	$-2H_2O$
		312	21.02 (20.54)	$-C_2H_5OCS_2$
		620	41.24 (40.29)	$-C_{15}H_{12}N_2OH$
10	$[Pr(C_2H_5OCS_2)(C_{15}H_{12}N_2O\cdot OCH_3)(2H_2O)Cl]\cdot H_2O$	87	3.11 (2.90)	$-H_2O$
		200	5.85 (5.73)	$-Cl$
		201	6.04 (5.81)	$-2H_2O$
		317	18.94 (19.55)	$-C_2H_5OCS_2$
		623	43.84 (43.14)	$-C_{16}H_{15}N_2O_2$
11	$[Pr(C_2H_5OCS_2)(C_{15}H_{12}N_2O\cdot CH_3)(2H_2O)Cl]\cdot H_2O$	86	3.12 (2.98)	$-H_2O$
		202	6.14 (5.88)	$-Cl$
		204	6.14 (5.97)	$-2H_2O$
		315	20.91 (20.06)	$-C_2H_5OCS_2$
		619	42.27 (41.63)	$-C_{16}H_{15}N_2O$
12	$[Pr(C_2H_5OCS_2)(C_{15}H_{12}N_2O\cdot Cl)(2H_2O)Cl]\cdot H_2O$	84	3.02 (2.88)	$-H_2O$
		201	5.81 (5.69)	$-Cl$
		202	5.89 (5.77)	$-2H_2O$
		318	20.17 (19.41)	$-C_2H_5OCS_2$
		621	44.12 (43.63)	$-C_{15}H_{12}N_2OCl$

complex 10 can also be justifies by the fact that excited electron delocalization occurs in these type of mixed ligand complexes. The $d\pi$–$d\pi$ back bonding of the sulfur donor ligand enhances the delocalization, and thus the life time increases.

The decrease in life time in complex 6 can be explained by results found in the literature,[87] in which the localization of energy states occur because of the presence of nitrogen. Because of increase in the number of nitrogen atoms, localization increases, the back bonding decreases, and thus, the energy increases. Because of this increased energy, the stability decreases, and thus, the life time also decreases. The lowest value of life time and the highest value of K_{nr} in complex 6 shows the maximum contribution of the non-radiative process in the excited state deactivation of the Pr ion.[82]

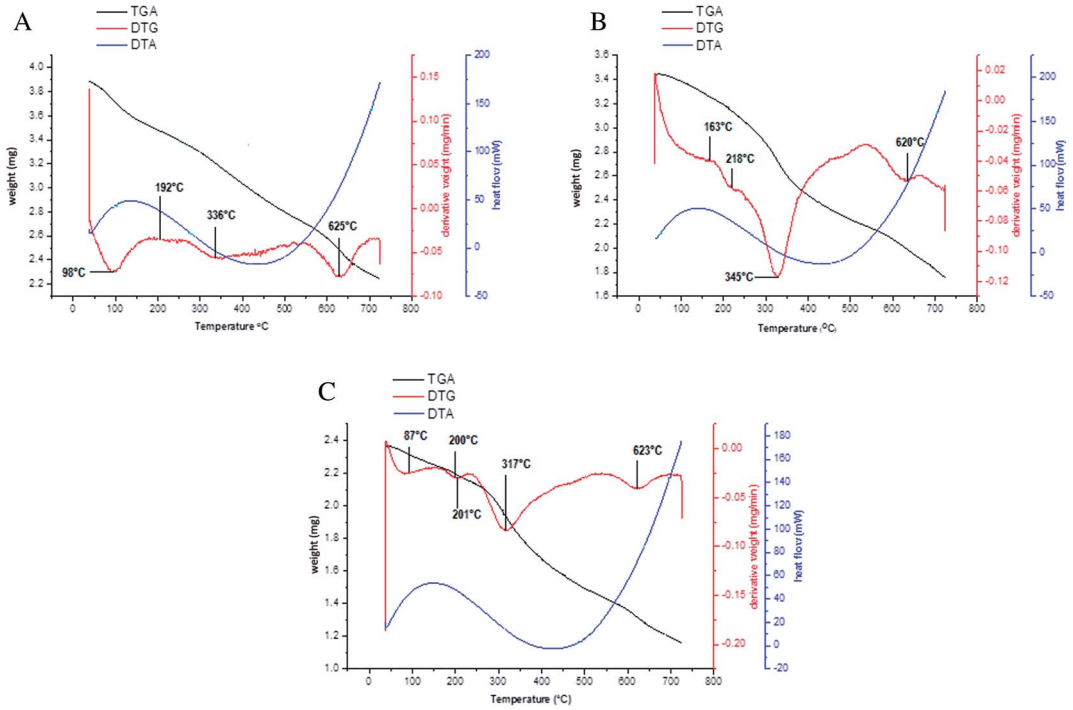

Fig. 4 (a) Decomposition pattern of $[Pr(C_{15}H_{12}N_2OH)(6H_2O)Cl_2].1.5H_2O$. (b) Decomposition pattern of $[Pr(C_5H_{10}NS_2)(C_{15}H_{12}N_2O{\cdot}OCH_3)(3H_2O)Cl]$. (c) Decomposition pattern of $[Pr(C_2H_5OCS_2)(C_{15}H_{12}N_2O{\cdot}OCH_3)(2H_2O)Cl]{\cdot}H_2O$.

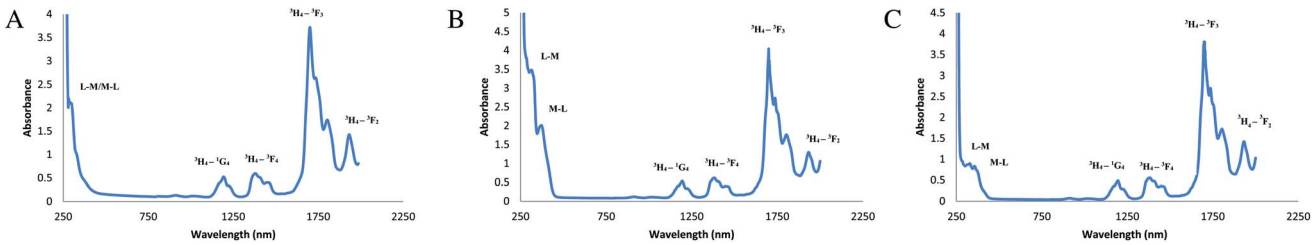

Fig. 5 (a) Absorption spectra of $[Pr(C_{15}H_{12}N_2OH)(6H_2O)Cl_2].1.5H_2O$, (b) absorption spectra of $[Pr(C_5H_{10}NS_2)(C_{15}H_{12}N_2O{\cdot}OCH_3)(3H_2O)Cl]$, (c) absorption spectra of $[Pr(C_2H_5OCS_2)(C_{15}H_{12}N_2O{\cdot}OCH_3)(2H_2O)Cl]{\cdot}H_2O$.

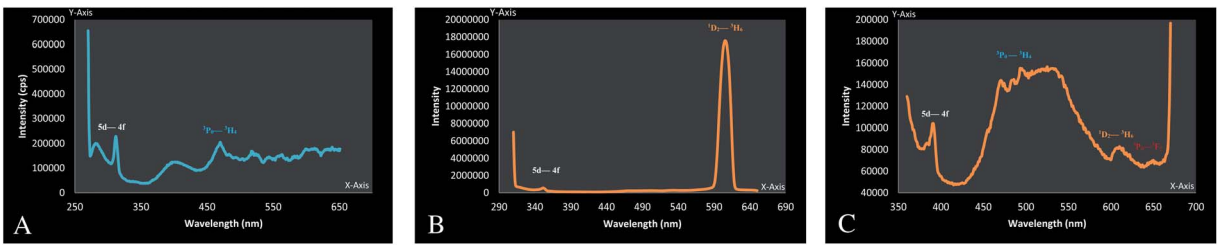

Fig. 6 (a) Emission spectra of $[Pr(C_{15}H_{12}N_2OH)(6H_2O)Cl_2]{\cdot}1.5H_2O$, (b) emission spectra of $[Pr(C_5H_{10}NS_2)(C_{15}H_{12}N_2O{\cdot}OCH_3)(3H_2O)Cl]$, (c) emission spectra of $[Pr(C_2H_5OCS_2)(C_{15}H_{12}N_2O{\cdot}OCH_3)(2H_2O)Cl]{\cdot}H_2O$.

The absorbed energy transferred by the ligand to the metal ion takes place from the ligand centered triplet excited state, which involves the sensitization for the Pr complexes.[82,88] Therefore, it can be seen that the selective tuning of the praseodymium emission can be obtained by changing the ligand's triplet state energy.[79] A strong red shift in absorption and emission maxima was obtained in complex 6 (when compared to other complexes) and a large Stoke's shift indicated that there was large nuclear distortion between the ground and excited singlet state and this lead to a low quantum

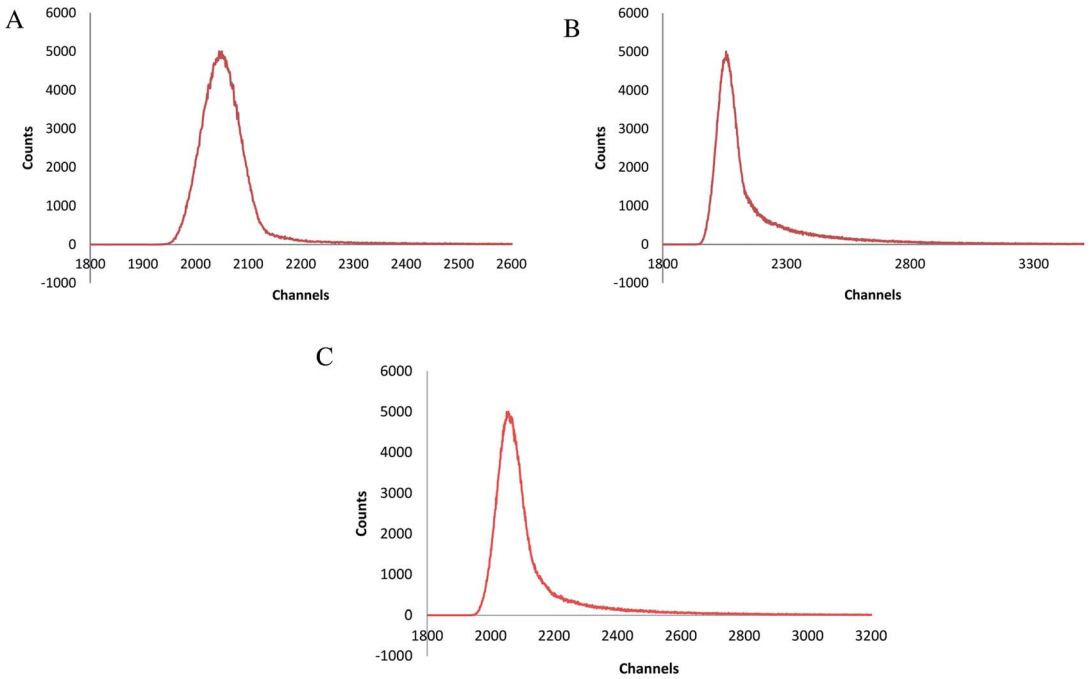

Fig. 7 (a) Emission lifetime spectra of $[Pr(C_{15}H_{12}N_2O\cdot H)(6H_2O)Cl_2]\cdot 1.5H_2O$, (b) emission lifetime spectra of $[Pr(C_5H_{10}NS_2)(C_{15}H_{12}N_2O\cdot OCH_3)(3H_2O)Cl]$, (c) emission lifetime spectra of $[Pr(C_5H_{10}NS_2)(C_{15}H_{12}N_2O\cdot OCH_3)(2H_2O)Cl]\cdot H_2O$.

Table 5 Luminescence characteristics of some representative complexes

Comp. no.	Complexes	Absorption (nm)	Excitation (nm)	Emission (nm)	Stoke's shift (nm)	K_r ($\times 10^6$ s^{-1})	K_{nr} ($\times 10^6$ s^{-1})	Φ	τ (ns)	Band gap (eV)
1	$[Pr(C_{15}H_{12}N_2O\cdot H)(6H_2O)Cl_2].1.5H_2O$	277	260	311	34	10.05	1.23	0.89	88.95	3.80
6	$[Pr(C_5H_{10}NS_2)(C_{15}H_{12}N_2O\cdot OCH_3)(3H_2O)Cl]$	334	310	604	270	7.38	6.04	0.55	74.48	3.87
10	$[Pr(C_2H_5OCS_2)(C_{15}H_{12}N_2O\cdot OCH_3)(2H_2O)Cl]\cdot H_2O$	357	340	389	32	8.73	0.86	0.91	104.18	3.65

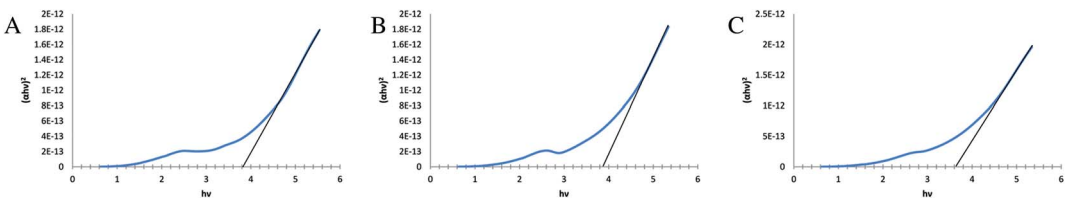

Fig. 8 (a) Tauc plot obtained for the complex $[Pr(C_{15}H_{12}N_2O\cdot H)(6H_2O)Cl_2]\cdot 1.5H_2O$ showing the band gap at 3.80 eV, (b) Tauc plot obtained for the complex $[Pr(C_5H_{10}NS_2)(C_{15}H_{12}N_2O\cdot OCH_3)(3H_2O)Cl]$ showing the band gap at 3.87 eV, (c) Tauc plot obtained for the complex $[Pr(C_2H_5OCS_2)(C_{15}H_{12}N_2O\cdot OCH_3)(2H_2O)Cl]\cdot H_2O$ showing the band gap at 3.65 eV.

yield and comparatively shorter life time.[89,90] The vibrational relaxation process of excited states in the Pr complexes 1 and 10 was justified by the small Stoke's shift, high quantum yield and a long life time shown by these complexes which was facilitated by the ligand behavior.[78] The high K_{nr} was caused by the lower emission energy and this high K_{nr} decreases the life time which is rationalized by the ligand oscillator.[80,91–96] All these luminescence characteristics of Pr complexes are given in Table 5. Band gaps of some Pr complexes were calculated using the Tauc plot shown in Fig. 8(a)–(c).

Overall the newly synthesized complexes show high quantum yield with a moderate life time and good value of band gap, thus, this could be used as a semiconductor in light emitting diodes such as gallium nitrides.

3.5 XRD, SEM and TEM studies

The complexes were found to be amorphous solids using X-ray diffraction studies (XRD) studies. The morphology of these Pr(III) complexes was studied using XRD, SEM and TEM. The

Table 6 PXRD, SEM and TEM analysis data of some representative complexes

Comp. no.	Compounds	Crystallite size (by XRD)	Average diameter (by SEM)	Average diameter (by TEM)
1	$[Pr(C_{15}H_{12}N_2O\cdot H)(6H_2O)Cl_2]\cdot 1.5H_2O$	40.81 nm	4.09 μm	2.17 nm
6	$[Pr(C_5H_{10}NS_2)(C_{15}H_{12}N_2O\cdot OCH_3)(3H_2O)Cl]$	40.85 nm	2.72 μm	1.03 nm
10	$[Pr(C_2H_5OCS_2)(C_{15}H_{12}N_2O\cdot OCH_3)(2H_2O)Cl]\cdot H_2O$	67.14 nm	2.27 μm	1.05 nm

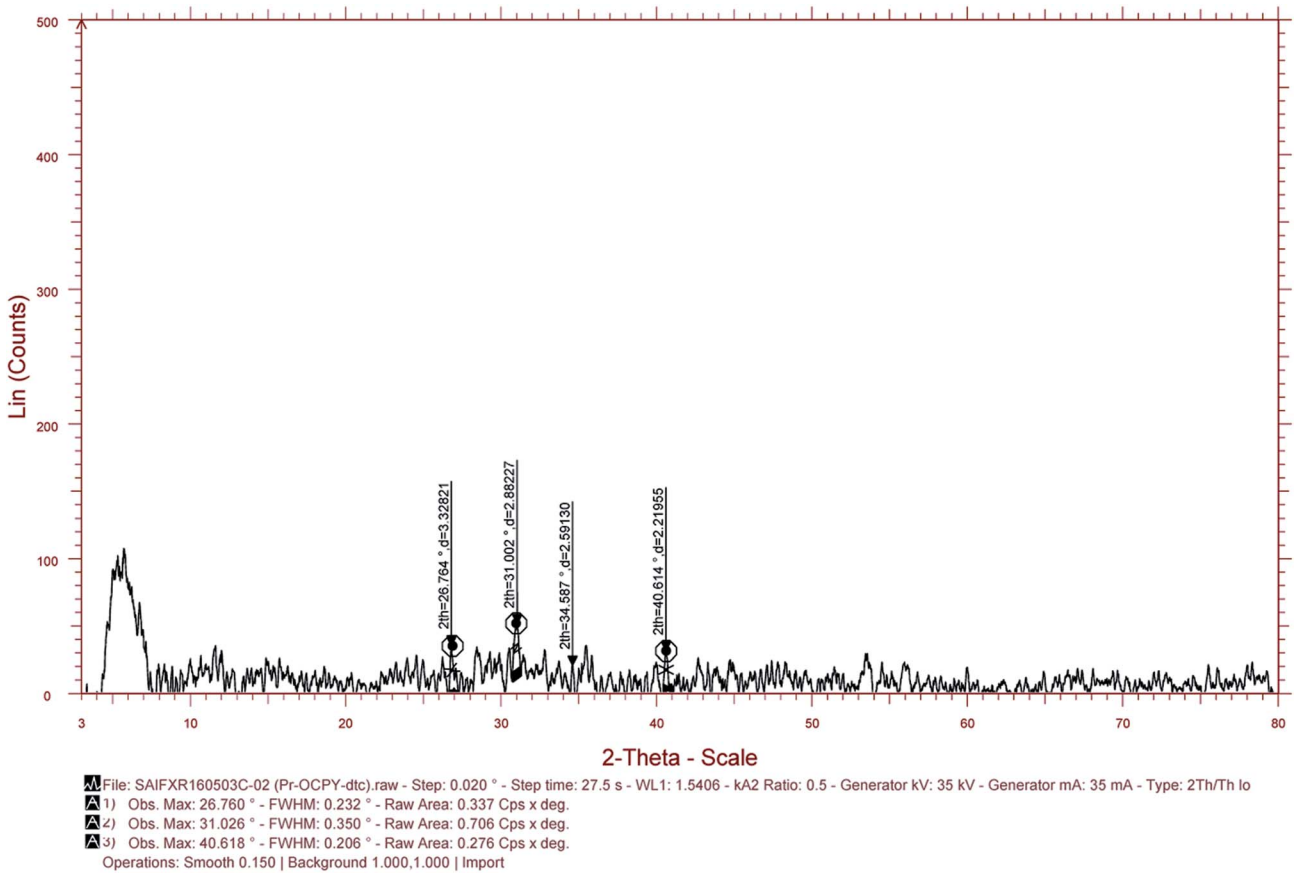

Fig. 9 PXRD peaks of $[Pr(C_5H_{10}NS_2)(C_{15}H_{12}N_2O\cdot OCH_3)(3H_2O)Cl]$.

crystallite sizes measured using XRD were near to nano size. The sizes of the crystals were calculated using the Debye–Scherrer equation with the full width at half maximum value (FWHM) value, obtained from the PXRD peaks. The variation in the size obtained using the PXRD method can be explained by calculating the particle size with different FWHM values for the different peaks that appeared in the PXRD graph. SEM and TEM images were used to observe the morphology of the particle and to determine the sizes of the inner core shell. PXRD data and TEM images of these particles show that these complexes are in the range nanometers. The SEM images show a somewhat larger size for these particles. The large size can be explained by intermolecular hydrogen bonding which results in associated molecules of large particle size at the surface. The particle size obtained using TEM was smaller because of minimum exposure to the environment. The sizes of some complexes are given in Table 6. The XRD peaks, SEM images of one of the complexes,

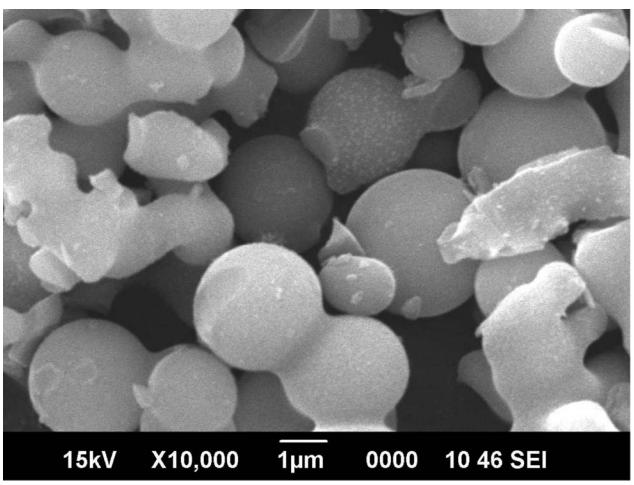

Fig. 10 SEM image of $[Pr(C_5H_{10}NS_2)(C_{15}H_{12}N_2O\cdot OCH_3)(3H_2O)Cl]$.

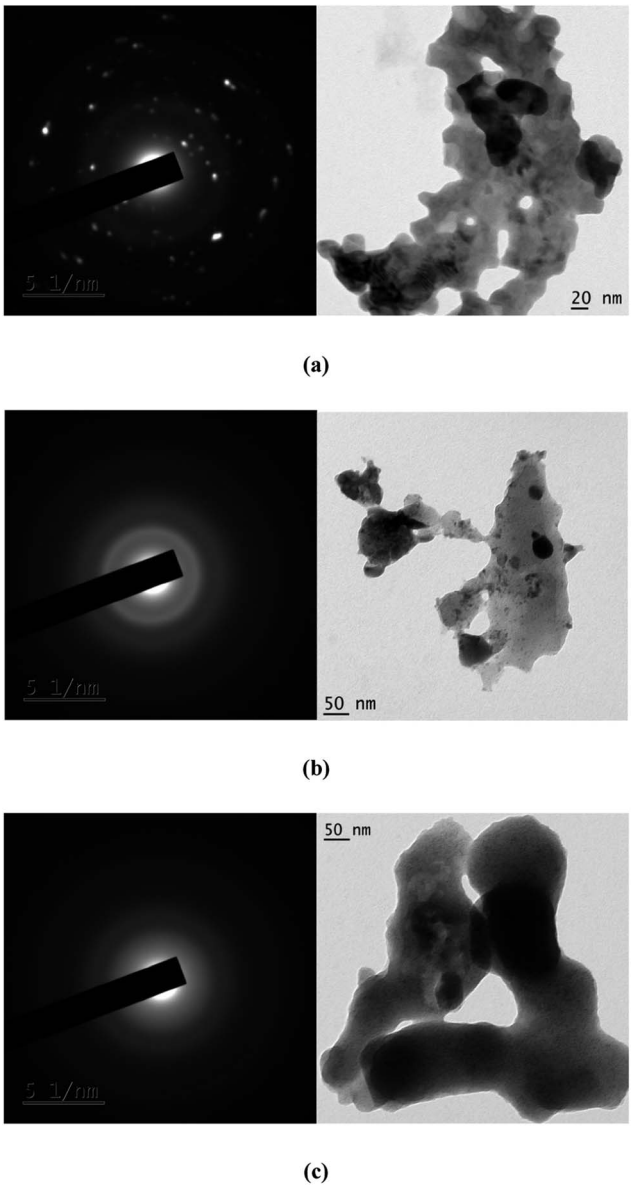

Fig. 11 SAED and TEM images of complex 2 (a), 6 (b) and 10 (c) showing the nature and sizes of the crystallite.

complex 6, are given in Fig. 9 and 10. The selected area electron diffraction (SAED) pattern and TEM images of some complexes showing the texture and sizes of crystallites, is augmented in Fig. 11.

3.6 Biological studies

The Pr complexes were tested against some bacteria, *P. aeruginosa*, *E. coli* and *S. aureus* and fungi *C. albicans*, and *A. niger*. The study shows variable screened results. Complex 6 gives maximum inhibition of growth (25.0 mm) against *P. aeruginosa* compared to the other two complexes, respective ligands and metal chloride, whereas complex 10 shows minimum inhibition of growth (12.0 mm) against the same bacteria when compared to their ligands and metal chloride. On complexation of metal chloride with the pyrazoline ligand, the antibacterial activity decreases to some extent. However, upon formation of mixed ligand complexes, the antibacterial activity decreases with complex 10, but noticeably increases with complex 6 (in *E. coli* and *P. aeruginosa*). The antibacterial activity of this type of complex decreases with *S. aureus*. When comparing the antibacterial activity of these complexes, ligands and metal chlorides with specific species, it was found that, for *E. coli*, complex 6 and its metal chloride showed maximum inhibition of bacterial growth (18.0 mm). The minimum inhibition zone (diameter of inhibition of growth) was found with complex 10. For *P. aeruginosa*, the maximum zone of inhibition was found with complex 6, whereas the lowest antibacterial activity was found with complex 10 and the OCH_3Py pyrazoline ligand. Metal chlorides showed maximum antibacterial activity with *S. aureus*, whereas the minimum activity is found with complex 10 and the dithiocarbamate ligand. Overall it was shown that all the complexes showed good antibacterial activity and they can be used as antibacterial drug for the same infections as tetracycline [Tables 7–10]. A comparative chart showing the antibacterial activity against these three pathogens is presented in Fig. 12.

Analysis of antifungal activity of complexes 2, 6 and 10 found that all show antifungal activity against *C. albicans* only, which manifests its selective action property. The observed results against *C. albicans* show that complex 2 gives the maximum zone of inhibition of 20 mm compared to complexes 6 and 10. Comparing the complexes with their respective ligands, it was found that complex 2 showed enhanced antifungal activity, whereas for the mixed ligand complexes 6 and 10, the antifungal activity was suppressed on complexation. Therefore, it can be noted here that on hydrolysis these complexes can show enhanced antifungal activity. All these ligands and complexes show somewhat lower antifungal activity in comparison to the drug fluconazole and can be used as mild antifungal agents. It may also be

Table 7 Antibacterial activity of complex 2, in comparison with the ligand and other mixed ligand complexes of praseodymium and tetracycline (a known antibacterial drug)

		Zone of inhibition (mm)				
Comp. no.	Pathogen	Complex 2	OCH_3Py	Complex 6	Complex 10	Tetracycline
1	*E. coli*	17.0	14.5	18.0	13.0	13.5
2	*P. aeruginosa*	14.0	12.5	25.0	12.0	13.0
3	*S. aureus*	16.5	14.5	12.0	16.5	13.5

Table 8 Antibacterial activity of Pr-OCPy-dtc in comparison with the ligands and another mixed ligand complex of praseodymium and tetracycline (a known antibacterial drug)

		Zone of inhibition (mm)				
Comp. no.	Pathogen	Complex 6	OCH3Py	dtc	Complex 10	Tetracycline
1	*E. coli*	18.0	14.5	15.0	13.0	13.5
2	*P. aeruginosa*	25.0	12.5	18.5	12.0	13.0
3	*S. aureus*	12.0	14.5	12.5	16.5	13.0

Table 9 Antibacterial activity of Pr-OCPy-Xan in comparison with the ligands and another mixed ligand complex of praseodymium and tetracycline (a known antibacterial drug)

		Zone of inhibition (mm)				
Comp. no.	Pathogen	Complex 10	OCH_3Py	Xanthate	Complex 6	Tetracycline
1	*E. coli*	13.0	14.5	16.5	18.0	13.0
2	*P. aeruginosa*	12.0	12.5	12.5	25.0	13.0
3	*S. aureus*	16.5	14.5	15.0	12.0	13.5

Table 10 Antibacterial activity of complex 2 (1), complex 6 (2) and complex 10 (3) in comparison with metal chloride and tetracycline (a known antibacterial drug)

		Zone of inhibition (mm)				
Comp. no.	Pathogen	1	2	3	$PrCl_3 \cdot 6H_2O$	Tetracycline
1	*E. coli*	17.0	18.0	13.0	18.0	13.0
2	*P. aeruginosa*	14.0	25.0	12.0	19.5	13.0
3	*S. aureus*	16.5	12.0	16.5	20.0	13.5

noted here that all the ligands and complexes have lesser antifungal activity than its metal chloride. The metal chloride shows a maximum zone of inhibition of 23.0 mm against both the fungi species [Tables 11–14]. A representative chart for antifungal activity against *C. albicans* and *A. niger* pathogens is given in Fig. 13.

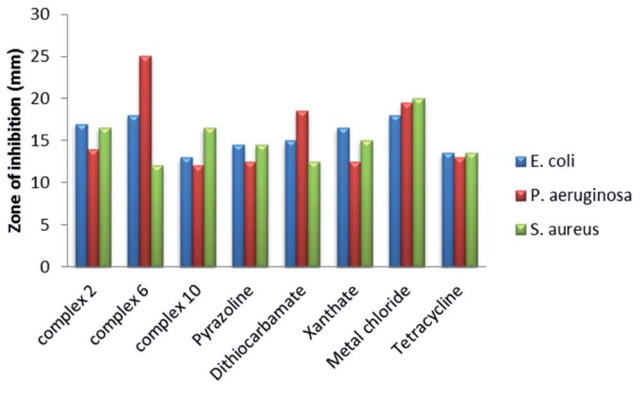

Fig. 12 Comparative chart for *in vitro* antibacterial activity compared to that of the standard drug tetracycline.

4 Conclusions

This paper describes the detailed study of a series of complexes of Pr(III) of the types $[Pr(C_{15}H_{12}N_2OX)(6H_2O)Cl_2]\cdot 1.5H_2O$, $[Pr(C_5H_{10}NS_2)(C_{15}H_{12}N_2OX)(3H_2O)Cl]$ and $[Pr(C_2H_5OCS_2)(C_{15}H_{12}N_2OX)(2H_2O)Cl]\cdot H_2O$. The IR spectral data indicates the bidentate mode of coordination of pyrazoline, dithiocarbamate and xanthate ligands. The XRD, SEM and TEM studies show the size of the particles. The TGA/DTG/DSC analyses confirmed the presence of water molecules. The elemental analysis showed the monomeric nature of these complexes. DART mass spectrometry confirmed the isotopic variation of chlorine in the complexes. Using all these facts together, the ligancy of these complexes were found to be: 10 (ref. 97) in complex 1, 8 (ref. 79 and 98) in complex 6 and 7 (ref. 79) in complex 10. The most likely geometry around the praseodymium(III) atom was a bicapped square, antiprism: D_4d (1), cubic: Oh (6) and capped trigonal prism: C_{2v} (10).

According to the photo-physical studies, the emission life time of these praseodymium complexes was highest for complex 10 which has the lowest coordination number of 7, whereas complexes 1 and 6 have nearly the same emission life time values. The reason behind this could be the presence of water and change in ligancy and environment around the praseodymium metal.

From the present study, the following important points can be concluded:

(i) Complex 1 has the highest K_r and moderate quantum yield (Φ), K_{nr}, Stoke's shift, emission life time and band gap.

Table 11 Antifungal activity of complex 2 in comparison with the ligand and other mixed ligand complexes of praseodymium and fluconazole (a known antifungal drug)

		Zone of inhibition (mm)				
Comp. no.	Pathogen	Complex 2	OCH_3Py	Complex 6	Complex 10	Fluconazole
1	*C. albicans*	20.0	19.0	13.0	15.0	21.5
2	*A. niger*	—	—	—	—	21.5

Table 12 Antifungal activity of complex 6 in comparison with the ligands and another mixed ligand complex of praseodymium and fluconazole (a known antifungal drug)

		Zone of inhibition (mm)				
Comp. no.	Pathogen	Complex 6	OCH_3Py	dtc	Complex 10	Fluconazole
1	*C. albicans*	13.0	19.0	16.0	15.0	21.5
2	*A. niger*	—	—	—	—	21.5

Table 13 Antifungal activity of complex 10 in comparison with the ligands and another mixed ligand complex of praseodymium and fluconazole (a known antifungal drug)

		Zone of inhibition (mm)				
Comp. no.	Pathogen	Complex 10	OCH3Py	Xanthate	Complex 6	Fluconazole
1	*C. albicans*	15.0	19.0	18.5	13.0	21.5
2	*A. niger*	—	—	—	—	21.5

Table 14 Antifungal activity of complex 2 (1), complex 6 (2) and complex 10 (3) in comparison with metal chloride and fluconazole (a known antifungal drug)

		Zone of inhibition (mm)				
Comp. no.	Pathogen	1	2	3	$PrCl_3 \cdot 6H_2O$	Fluconazole
1	*C. albicans*	20.0	13.0	15.0	23	21.0
2	*A. niger*	—	—	—	23	21.0

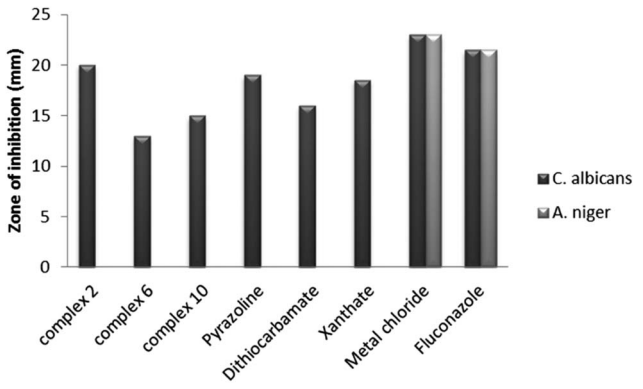

Fig. 13 Comparative chart for *in vitro* antifungal activity compared to that of the standard drug fluconazole.

(ii) Complex 6 has the highest value of Stoke's shift and band gap and the lowest value of quantum yield and emission life time.

(iii) Complex 10 has the highest emission life time and quantum yield, the lowest K_{nr}, Stoke's shift and band gap and a moderate K_r.

(iv) Complex 6 has almost the same radiative and non-radiative decay rate, whereas complexes 1 and 10 have a much lower non-radiative decay rate than the radiative decay rate.

(v) The antimicrobial studies reveal that these Pr(III) complexes can act as good antibacterial and mild antifungal drugs.

Conflicts of interest

There are no conflicts of interest to declare.

Abbreviations

DART	Direct analysis in real time
DTA	Differential thermal analysis
dtc	Sodium diethyldithiocarbamate $[Na(C_5H_{10}NS_2)] \cdot 3H_2O$
DTG	Differential thermal analysis
FTIR	Fourier-transform infrared spectroscopy

OCH_3Py	3(2′-Hydroxyphenyl)-5-(4-methoxyphenyl) pyrazoline, $[C_{15}H_{13}N_2O{\cdot}OCH_3]$
$PrCl_3{\cdot}6H_2O$	Praseodymium chloride
Pr-OCH_3Py	Complex 2; $[Pr(C_{15}H_{12}N_2O{\cdot}OCH_3)(6H_2O)Cl_2]{\cdot}1.5H_2O$
Pr-OCPy-dtc	Complex 6; $[Pr(C_5H_{10}NS_2)(C_{15}H_{12}N_2O{\cdot}OCH_3)(3H_2O)Cl]$
Pr-OCPy-Xan	Complex 10; $[Pr(C_2H_5OCS_2)(C_{15}H_{12}N_2O{\cdot}OCH_3)(2H_2O)Cl]{\cdot}H_2O$
PXRD	Powder X-ray diffraction
SEM	Scanning electron microscopy
TEM	Transmission electron microscopy
TGA	Thermogravimetric analysis
UV-visible	Ultraviolet-visible spectroscopy
Xanthate	Potassium ethylxanthate $[K(C_2H_5OCS_2)]{\cdot}3H_2O$

Acknowledgements

The authors are grateful to the SAIF at CDRI (Lucknow, India), the SAIF at IIT Madras (India), and the STIC (Cochin, India) for providing the necessary spectral and analytical data. The authors also wish to thank the MRD LifeSciences (Lucknow) for proving the important biological studies. This work is financially supported by the UGC-BSR program [F. No. 25-1/2014-15/(BSR)/5-25/2007(BSR)]. We also wish to thank the Department of Chemistry, D. D. U. Gorakhpur University, Gorakhpur, India for providing the laboratory and library facilities.

References

1 W. D. Horrocks and D. R. Sudnick, *Acc. Chem. Res.*, 1981, **14**, 384.
2 N. Sabbatini, M. Guardigli and I. Manet, *Handbook of the Physics and Chemistry of Rare Earths*, Elsevier, Amsterdam, 1996.
3 D. Parker and J. A. Williams, *J. Chem. Soc., Dalton Trans.*, 1996, **18**, 3613.
4 K. Mohanan, N. Subhadrambika, R. S. Joseyphus, S. S. Swathy and V. P. Nisha, *J. Saudi Chem. Soc.*, 2016, **20**, 379.
5 Z. A. Taha, A. M. Ajlouni, K. A. Al-Hassan, A. K. Hijazi and A. B. Faiq, *Spectrochim. Acta, Part A*, 2011, **81**, 317.
6 I. Khan, Z. Mahmood and M. Naz, *Int. J. Chem. Stud.*, 2016, **4**, 17.
7 G. Karthikeyan, K. Mohanraj, K. P. Elango and K. Girishkumar, *Russ. J. Coord. Chem.*, 2006, **32**, 380.
8 F. Liu, S. Y. He, H. X. Li and F. Y. Chen, *Russ. J. Coord. Chem.*, 2010, **36**, 317.
9 L. Yang, D. Tao, X. Yang, Y. Li and Y. Guo, *Chem. Pharm. Bull.*, 2003, **51**, 494.
10 S. V. S. Babu and K. H. Reddy, *Iran. J. Chem. Chem. Eng.*, 2017, **36**, 101.
11 K. Mohanan, N. Subhadrambika, R. S. Joseyphus, S. S. Swathy and V. P. Nisha, *J. Saudi Chem. Soc.*, 2016, **20**, 379.
12 G. Karthikeyan, K. Mohanraj and K. P. Elango, *Transition Met. Chem.*, 2004, **29**, 86.
13 J. Pusz, E. Ciszkowicz, K. Lecka-Szlachta, S. Wolowiec and E. Woznicka, *Acta Pol. Pharm.*, 2017, **74**, 1101.
14 V. Geethalaksmi and C. Theivarasu, *Int. J. Chem. Sci.*, 2016, **14**, 910.
15 S. Shionoya and W. M. Yen, *Phosphor Handbook*, 1999, vol. 177.
16 V. W. W. Yam and K. K. W. Lo, *Coord. Chem. Rev.*, 1999, **184**, 157.
17 D. Parker, *Coord. Chem. Rev.*, 2000, **205**, 109.
18 T. J. Foley, B. S. Harrison, A. S. Knefely, K. A. Abboud, J. R. Reynolds, K. S. Schanze and J. M. Boncella, *Inorg. Chem.*, 2003, **42**, 5023.
19 F. C. J. M. Van Veggel, G. A. Hebbink, S. I. Klink, L. Grave and P. G. B. Oude Alink, *ChemPhysChem*, 2002, **3**, 1014.
20 S. Faulkner and S. J. A. Pope, *J. Am. Chem. Soc.*, 2003, **125**, 10526.
21 R. S. Dickins, S. Aime, A. S. Batsanov, A. Beeby, M. Botta, J. Bruce, J. A. K. Howard, C. S. Love, D. Parker, R. D. Peacock, H. Buschmann and S. Aime, *J. Am. Chem. Soc.*, 2002, **124**, 12697.
22 I. A. Kamenskikh, N. Guerrasimova, C. Dujardin, N. Garnier, G. Ledoux, C. Pedrini, M. Kirm, A. Petrosyan and D. Spassky, *Opt. Mater.*, 2003, **24**, 267.
23 W. K. Wong, H. Z. Liang, W. Y. Wong, Z. W. Cai, K. F. Li and K. W. Cheah, *New J. Chem.*, 2002, **26**, 275.
24 N. M. Shavaleev, S. J. A. Pope, Z. R. Bell, S. Faulkner and M. D. Ward, *Dalton Trans.*, 2003, 808.
25 Y. Oshishi, T. Kanamori, T. Kitagawa, S. Takashashi, E. Snitzer and G. H. Sigel Jr, *Opt. Lett.*, 1991, **16**, 1747.
26 L. H. Slooff, A. Polman, M. P. O. Wolbers, F. van Veggel, D. N. Reinhoudt and J. W. Hofstraat, *J. Appl. Phys.*, 1998, **83**, 497.
27 A. Kaminskii, *Laser crystals*, Springer, Moscow, 1990.
28 R. Moorty and M. Jagasin, *Mater. Chem. Phys.*, 2005, **93**, 455.
29 Y. K. Sharma, S. P. Tondon and S. S. L. Surana, *Mater. Sci. Eng., B*, 2000, **77**, 167.
30 Y. C. Ratnakaram, A. V. Kumar, D. T. Naidu and N. O. Gopal, *Mater. Lett.*, 2004, **58**, 3908.
31 A. Florez, O. L. Malta, Y. Messaddeq and M. Aegerter, *J. Non-Cryst. Solids*, 1997, **213–214**, 315.
32 K. Wei, D. P. Machewirth, J. Wenzel, E. Snitzer and G. H. Sigel Jr, *J. Non-Cryst. Solids*, 1995, **182**, 257.
33 N. Wang, W. Jiang, X. Xu, Z. Si, H. Bai and C. Tian, *Anal. Sci.*, 2002, **18**, 591.
34 A. Lecointre, A. Bessière, A. Bos, P. Dorenbos, B. Viana and S. Jacquart, *J. Phys. Chem. C*, 2011, **115**, 4217.
35 P. Boutinaud, L. Sarakha, E. Cavalli, M. Bettinelli, P. Dorenbos and R. Mahiou, *J. Phys. D: Appl. Phys.*, 2009, **42**, 045106.
36 P. Boutinaud, L. Sarakha and R. Mahiou, *J. Phys.: Condens. Matter*, 2009, **21**, 025901.
37 Y. F. Lin, Y. H. Chang, Y. S. Chang, B. S. Tsai and Y. C. Li, *J. Electrochem. Soc.*, 2006, **153**, G543.
38 L. Zhang, J. Liu, J. Gao, F. Zhang and L. Ding, *Molecules*, 2017, **22**, 1304.
39 D. Zhen-bo, S. T. Lee, C. Li-chun, D. Shu-zhong, S. Heng-hui and W. Xun, *Acta Phys. Sin.*, 1997, **6**, 921.
40 M. Liu and J. Zhang, *Heterocycl. Commun.*, 2016, **22**, 31.

41 Q. J. Liu, L. Gao, L. Wang, Z. Y. Xie and D. F. Li, *Spectrosc. Spectral Anal.*, 2009, **29**, 2810.
42 Y. F. Xian, D. F. Li and Y. M. Wang, *Spectrosc. Spectral Anal.*, 2008, **28**, 1617.
43 G. J. Pant, P. Singh, B. S. Rawat, M. S. M. Rawat and G. C. Joshi, *Spectrochim. Acta, Part A*, 2011, **78**, 1075.
44 J. Shun-Jun and S. Hai-Bin, *Dyes Pigm.*, 2006, **70**, 246.
45 B. Lu, J. Zhang, M. Wang, Y. Zhou and X. Chen, *Chin. J. Chem.*, 2012, **30**, 1345.
46 T. Suwunwong, S. Chantrapromma and H. K. Fun, *Opt. Spectrosc.*, 2015, **118**, 563.
47 A. I. Vogel, *A text book of quantitative organic analysis*, ELBS and Longman Group Ltd., London, 1978.
48 T. C. Sharma, V. Saxena and N. J. Readdy, *Helv. Chim. Acta*, 1977, **93**, 415.
49 J. E. Drake, C. L. B. McDonald, A. Kumar, S. K. Pandey and R. Ratnani, *J. Chem. Crystallogr.*, 2005, **35**, 447.
50 I. Ahmad and A. J. Beg, *J. Ethnopharmacol.*, 2001, **74**, 113.
51 S. Dash, L. K. Nath and S. Bhise, *Trop. J. Pharm. Res.*, 2005, **4**, 341.
52 A. I. Vogel, *Textbook of qualitative inorganic analysis*, Else and Longman, London, 1973.
53 C. J. Rodden, *J. Res. Natl. Bur. Stand.*, 1941, **26**, 557.
54 U. N. Tripathi, G. Venubabu, M. S. Ahmad, S. S. R. Kolisetty and A. K. Srivastav, *Appl. Organomet. Chem.*, 2006, **20**, 669.
55 U. N. Tripathi, M. S. Ahmad, G. Venubabu and D. R. Khate, *Main Group Met. Chem.*, 2006, **29**, 39.
56 U. N. Tripathi, G. Venubabu, M. S. Ahmad and P. Ramakrishna, *J. Coord. Chem.*, 2007, **60**, 1777.
57 U. N. Tripathi, G. Venubabu and M. S. Ahmad, *J. Coord. Chem.*, 2007, **60**, 1709.
58 U. N. Tripathi, G. Venubabu and M. S. Ahmad, *Turk. J. Chem.*, 2007, **31**, 45.
59 U. N. Tripathi, J. S. Solanki, A. Bhardwaj and T. R. Thapak, *J. Coord. Chem.*, 2008, **61**, 4025.
60 U. N. Tripathi, M. S. Ahmad, J. S. Solanki and A. Bhardwaj, *J. Coord. Chem.*, 2009, **62**, 636.
61 K. V. Sharma, V. Sharma and U. N. Tripathi, *J. Coord. Chem.*, 2008, **62**, 3314.
62 J. R. Ferraro, *Low frequency vibrations of inorganic and coordination compounds*, Plenum, New York, 1971.
63 K. Nakamoto, *Infrared Spectra of Inorganic and Coordination Compounds*, Wiley-Interscience, New York, 1970.
64 L. Zapala, M. Kosinska, E. Woznicka, L. Byczynski, W. Zapala and J. Kalembkiewicz, *J. Anal. Appl. Pyrolysis*, 2017, **123**, 1.
65 M. R. Anoop, K. R. Jisha, S. Suma and M. R. Sudarsanakumar, *J. Rare Earths*, 2014, **32**, 43.
66 L. Zapala, M. Kosińska, E. Woznicka, L. Byczynski and W. Zapala, *J. Therm. Anal. Calorim.*, 2016, **124**, 363.
67 N. Mahe, O. Guillou, C. Daiguebonne, Y. Gerault, A. Caneschi, C. Sangregorio, J. Y. Chane-Ching, P. E. Car and T. Roisnel, *Inorg. Chem.*, 2005, **44**, 7743.
68 M. I. Khalil, A. M. Al-Zahem and M. M. Qunaibit, *Med. Chem. Res.*, 2014, **23**, 1683.
69 F. X. Campos, A. L. C. S. Nascimento, T. A. D. Colman, D. A. Galico, O. Treu-Filho, F. J. Caires, A. B. Siqueira and M. Ionashiro, *J. Therm. Anal. Calorim.*, 2016, **123**, 91.
70 A. L. C. S. Nascimento, F. J. Caires, T. A. D. Colman, D. J. C. Gomes, G. Bannach and M. Ionashiro, *Thermochim. Acta*, 2015, **604**, 7.
71 A. L. C. S. Nascimento, J. A. Teixeira, W. D. G. Nunes, F. X. Campos, O. Treu-Filho, F. J. Caires and M. Ionashiro, *J. Anal. Appl. Pyrolysis*, 2016, **119**, 242.
72 L. C. V. Rodrigues, H. F. Brito, J. Holsa and M. Lastusaari, *Opt. Mater. Express*, 2012, **2**, 382.
73 B. Yan, W. Wan and Y. Song, *Spectrochim. Acta, Part A*, 2007, **66**, 1115.
74 G. H. Dieke, *Spectra and Energy Levels of Rare Earth Ions in Crystals*, Wiley-Interscience, New York, 1968.
75 S. Quici, M. Cavazzini, G. Marzanni, G. Accorsi, N. Armaroli, B. Ventura and F. Barigelletti, *Inorg. Chem.*, 2005, **44**, 529.
76 B. Zhou, L. Tao, Y. H. Tsang, W. Jin and E. Y. B. Pun, *J. Opt. Soc. Am.*, 2012, **20**, 3803.
77 A. I. Voloshin, N. M. Shavaleev and V. P. Kazakov, *J. Lumin.*, 2001, **93**, 199.
78 E. B. Sveshnikova and N. T. Timofeev, *Opt. Spectrosc.*, 1980, **48**, 503.
79 R. Kumar and U. P. Singh, *J. Coord. Chem.*, 2008, **61**, 2663.
80 H. Yin, P. J. Carroll, B. C. Manor, J. M. Anna and E. J. Schelter, *J. Am. Chem. Soc.*, 2016, **138**, 5984.
81 S. Cotton, *Lanthanide and Actinide Chemistry*, John Wiley and Sons, West Sussex, UK, 2006.
82 A. Dossing, A. Kadziola, P. Gawryszewska, A. Watras and A. Melchior, *Inorg. Chim. Acta*, 2017, **467**, 93.
83 V. P. Dotsenko, N. P. Efryushina and I. V. Berezovskaya, *Opt. Spectrosc.*, 1995, **79**, 105.
84 A. G. Svetashev and M. P. Tsvirko, *Zh. Prikl. Spektrosk.*, 1995, **62**, 249.
85 D. Manzania, D. Paboeuf, S. J. L. Ribeirao, P. Goldner and F. Bretenakerb, *Opt. Mater.*, 2013, **35**, 383.
86 M. D. Regulacio, M. H. Pablico, J. A. Vasquez, P. N. Myers, S. Gentry, M. Prushan, S. W. T. Chang and S. L. Stoll, *Inorg. Chem.*, 2008, **47**, 1512.
87 S. B. Bouzid, F. Bousbih, R. Chtourou and E. Tounie, *Solid State Commun.*, 2004, **130**, 121.
88 S. V. Eliseeva and J. C. G. Bunzli, *Chem. Soc. Rev.*, 2010, **39**, 189.
89 R. Hermann and R. Mehnert, *J. Lumin.*, 1985, **33**, 69.
90 W. Rothman, F. Hirayama and S. Lipsky, *J. Chem. Phys.*, 1970, **5**, 296.
91 W. R. Browne and J. G. Vos, *Coord. Chem. Rev.*, 2001, **219**, 761.
92 J. C. G. Bunzli and C. Piguet, *Chem. Soc. Rev.*, 2005, **34**, 1048.
93 S. Marks, J. G. Heck, M. H. Habicht, P. Ona-Burgos, C. Feldmann and P. W. J. Roesky, *J. Am. Chem. Soc.*, 2012, **134**, 16983.
94 J. C. G. Bunzli, *Coord. Chem. Rev.*, 2015, **293–294**, 19.
95 S. Yanagida, Y. Hasegawa, K. Murakoshi, Y. Wada, N. Nakashima and T. Yamanaka, *Coord. Chem. Rev.*, 1998, **171**, 461.
96 C. Doffek and M. Seitz, *Angew. Chem., Int. Ed.*, 2015, **54**, 9719.
97 I. A. Charushnikova and C. Den Auwer, *Crystallogr. Rep.*, 2006, **51**, 982.
98 G. Blasse, *Prog. Solid State Chem.*, 1988, **18**, 79.